ADVANCED ENERGY MATERIALS

# Supporting Information

for *Adv. Energy Mater.,* DOI: 10.1002/aenm.202100181

# Phase Boundary Mapping of Tin-Doped ZnSb Reveals Thermodynamic Route to High Thermoelectric Efficiency

*Maxwell Wood, Michael Y. Toriyama, Shristi Dugar, James Male, Shashwat Anand, Vladan Stevanović, and G. Jeffrey Snyder**

# Supporting Information

## Phase Boundary Mapping of Tin-Doped ZnSb Reveals Thermodynamic Route to High Thermoelectric Efficiency

Max Wood,†[ab] Michael Y. Toriyama,†[a] Shristi Dugar,†[a] James Male,[a] Shashwat Anand,[a] Vladan Stevanović,[c] and G. Jeffrey Snyder*[a]

a. *Northwestern University, Evanston, IL 60208, USA.*
b. *Jet Propulsion Laboratory, California Institute of Technology, Pasadena, California 91109, USA*
c. *Colorado School of Mines, Golden, CO 80401, USA.*

† These authors contributed equally to this work.

E-mail: jeff.snyder@northwestern.edu

## DFT Phase Diagram and Formation Energies

The formation enthalpies of compounds in the Zn-Sb-Sn ternary phase space, calculated using DFT, are listed in Table S1. The formation enthalpies yield a phase diagram (Figure S1) which is quite similar to the experimentally-determined one.

Table S1. Formation energies of compounds constituting the three-phase regions shown in the Zn-Sn-Sb phase diagram in Figure S1. Fitted elemental reference energies[21] are used as the intrinsic atomic chemical potentials of Zn, Sb, and Sn to calculate the formation energies.

| | ZnSb | $ZnSnSb_2$ | $Zn_{13}Sb_{10}$ | SnSb |
|---|---|---|---|---|
| Formation Energy (eV/atom) | -0.130 | -0.116 | -0.125 | -0.0106 |

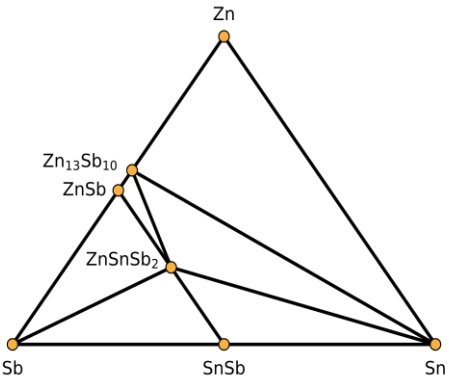


Figure S1. The Zn-Sb-Sn phase diagram calculated using DFT, according to the formation energies shown in Table S1.

The relationship between the atomic chemical potentials and the formation enthalpies of impurity phases can be visualized diagrammatically using the convex hull construction, as exemplified for the Zn-Sb binary composition axis in Figure S2. A lower formation enthalpy of $Zn_{13}Sb_{10}$ with respect to solid Zn and Sb corresponds to a lower Zn chemical potential and higher Sb chemical potential (blue line) compared to a hypothetically higher formation enthalpy of $Zn_{13}Sb_{10}$ (red line). Uncertainties in the formation enthalpies of impurity phases will therefore correspond directly to uncertainties in the atomic chemical potentials and, perhaps more importantly, the defect formation energies. It is therefore worth exploring discrepancies between the Zn-Sb-Sn ternary phase

diagrams at 0 K (Figure S1) and 400°C (Figure 2) in order to link the calculated defect energetics and the experimentally-measured Hall carrier concentrations.

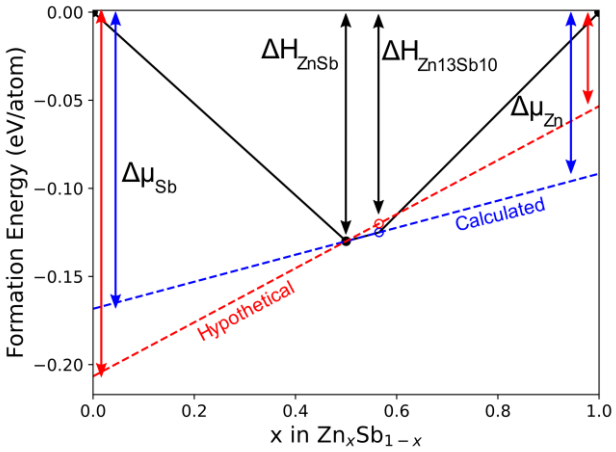


Figure S2. The Zn-Sb binary convex hull, depicting the influence of the formation energy of $Zn_{13}Sb_{10}$ on the atomic chemical potential of Zn and Sb. The diagram is relevant when ZnSb is in equilibrium with $Zn_{13}Sb_{10}$ and one other phase (e.g. ZnSb-$Zn_{13}Sb_{10}$-Sn, or phase region 4). The atomic chemical potentials of Zn and Sb in such a three-phase region are the intercepts of the tangent line connecting ZnSb to $Zn_{13}Sb_{10}$. The blue line relates the actual DFT-calculated formation enthalpy of $Zn_{13}Sb_{10}$ to the atomic chemical potentials of Zn and Sb. The red line demonstrates the hypothetical situation in which the formation enthalpy of $Zn_{13}Sb_{10}$ is slightly higher. In the latter case, the Zn and Sb chemical potentials are higher and lower, respectively, compared to the potentials when the formation enthalpy of $Zn_{13}Sb_{10}$ is lower.

The DFT phase diagram posits that $Zn_{13}Sb_{10}$ is a stable impurity phase, breaking the Zn-Sb binary convex hull by ≈12 meV/atom. Previous studies however suggest that β-$Zn_4Sb_3$ is barely stable under experimental conditions. First-principles defect calculations have found that the Zn vacancy has a negative formation energy in β-$Zn_4Sb_3$, which may suggest that the compound is metastable against a Zn-deficient compound close in composition. β-$Zn_4Sb_3$ additionally stabilizes against decomposition into Zn and ZnSb through entropy, suggesting that temperature effects must be addressed to accurately describe its thermodynamic stability. Therefore, the considerably low formation energy of $Zn_{13}Sb_{10}$ from our 0 K calculation may be *overestimating* the stability of the $Zn_{13}Sb_{10}$ compound. $ZnSnSb_2$ additionally undergoes an order-disorder transition between 225 and 240°C, as well as a peritectic decomposition at 360°C. As a result, the experimentally-measured phase diagram at 400°C may involve entropic contributions that are not treated explicitly in our DFT calculations. There may also be a discrepancy in the Sn elemental reference potential, since the Sn phase at 400°C is in a liquid state. The uncertainties surrounding the inherent 0 K description of DFT as a result account for discrepancies in the experimental and DFT phase diagrams. For example, a tie line between $Zn_{13}Sb_{10}$ and $ZnSnSb_2$ is present in the DFT phase diagram (Figure S1) and absent from the experimental phase diagram (Figure 2).

Due to such uncertainties related to temperature effects in the system, perhaps one way to interpret the DFT results as a predictive tool would be to study the three-phase regions similar to those that appear in the experimental phase diagram. Additionally, since carrier concentrations from DFT calculations seldom match those measured experimentally, we believe it is more instructive to study the ratio of the calculated carrier concentrations in the Zn-rich (corresponding to experimental phase regions 3 or 4) and Sb-rich (corresponding to phase regions 1 or 2) sides. As shown, the calculated carrier concentrations in the ZnSb-Zn-Sn, ZnSb-$Zn_{13}Sb_{10}$-Sn, and ZnSb-$ZnSnSb_2$-Sn three-phase regions is $\approx 2 \cdot 10^{20}$ $cm^{-3}$, whereas the carrier concentrations in the ZnSb-$ZnSnSb_2$-Sb, ZnSb-SnSb-Sb, and ZnSb-SnSb-Sn regions is $\approx 4 \cdot 10^{19}$ $cm^{-3}$. Our results therefore predict a 5-fold increase in carrier concentration when synthesizing samples under different conditions. Despite the uncertainties in projecting the inherently 0 K description of DFT to finite-temperature observations, our results nevertheless elucidate key features of phase boundary mapping and its importance in tuning the carrier concentration of a material.

## Defect Formation Energies in Different Phase Regions

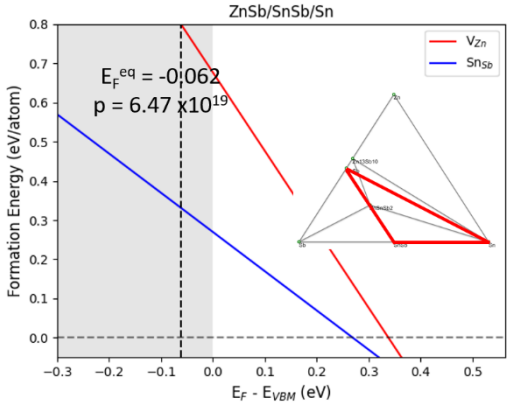
ZnSb/SnSb/Sn
$E_F^{eq}$ = -0.062
p = 6.47 x10$^{19}$
$V_{Zn}$
$Sn_{Sb}$
Formation Energy (eV/atom)
$E_F$ - $E_{VBM}$ (eV)

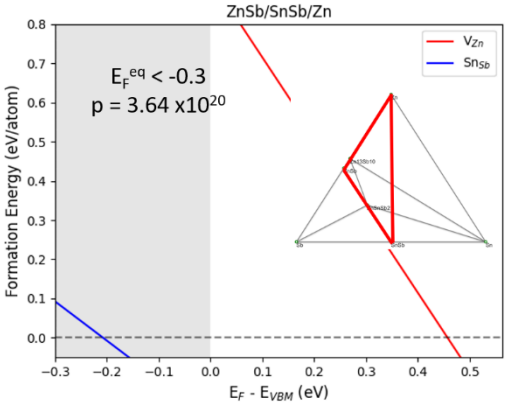
ZnSb/SnSb/Zn
$E_F^{eq}$ < -0.3
p = 3.64 x10$^{20}$
$V_{Zn}$
$Sn_{Sb}$
Formation Energy (eV/atom)
$E_F$ - $E_{VBM}$ (eV)

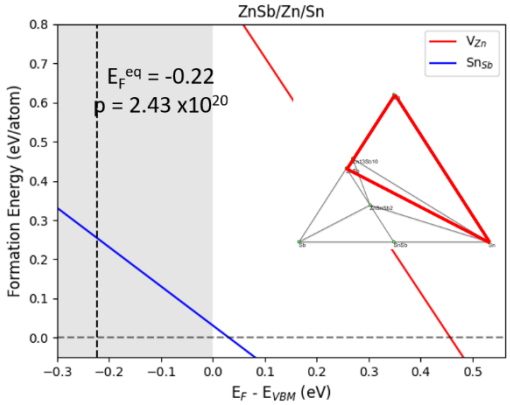
ZnSb/Zn/Sn
$E_F^{eq}$ = -0.22
p = 2.43 x10$^{20}$
$V_{Zn}$
$Sn_{Sb}$
Formation Energy (eV/atom)
$E_F$ - $E_{VBM}$ (eV)

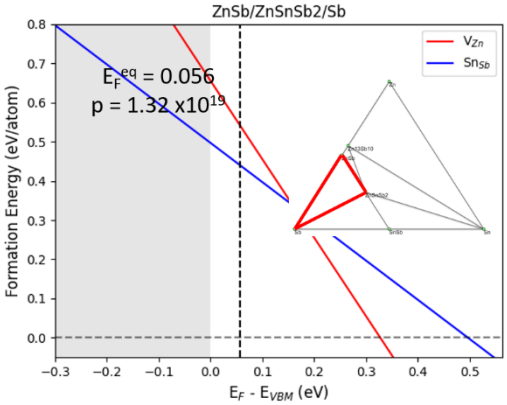
ZnSb/ZnSnSb2/Sb
$E_F^{eq}$ = 0.056
p = 1.32 x10$^{19}$
$V_{Zn}$
$Sn_{Sb}$
Formation Energy (eV/atom)
$E_F$ - $E_{VBM}$ (eV)

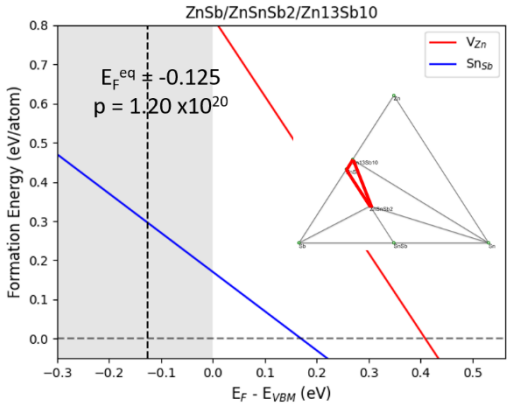
ZnSb/ZnSnSb2/Zn13Sb10
$E_F^{eq}$ = -0.125
p = 1.20 x10$^{20}$
$V_{Zn}$
$Sn_{Sb}$
Formation Energy (eV/atom)
$E_F$ - $E_{VBM}$ (eV)

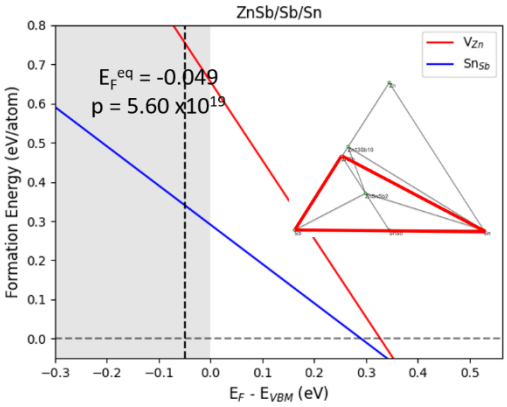
ZnSb/Sb/Sn
$E_F^{eq}$ = -0.049
p = 5.60 x10$^{19}$
$V_{Zn}$
$Sn_{Sb}$
Formation Energy (eV/atom)
$E_F$ - $E_{VBM}$ (eV)

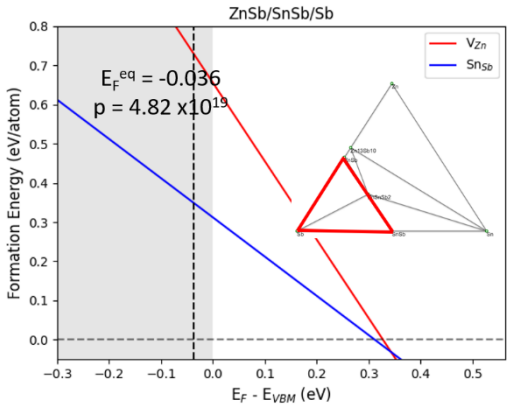
ZnSb/SnSb/Sb
$E_F^{eq}$ = -0.036
p = 4.82 x10$^{19}$
$V_{Zn}$
$Sn_{Sb}$
Formation Energy (eV/atom)
$E_F$ - $E_{VBM}$ (eV)

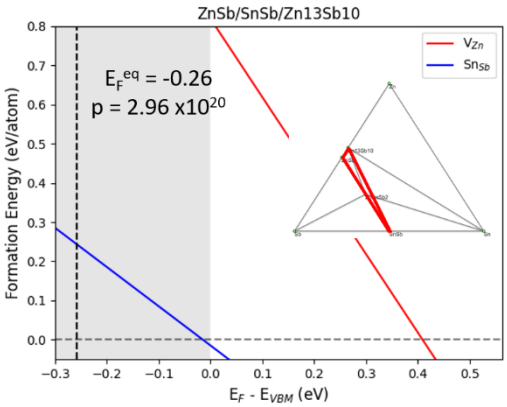
ZnSb/SnSb/Zn13Sb10
$E_F^{eq}$ = -0.26
p = 2.96 x10$^{20}$
$V_{Zn}$
$Sn_{Sb}$
Formation Energy (eV/atom)
$E_F$ - $E_{VBM}$ (eV)

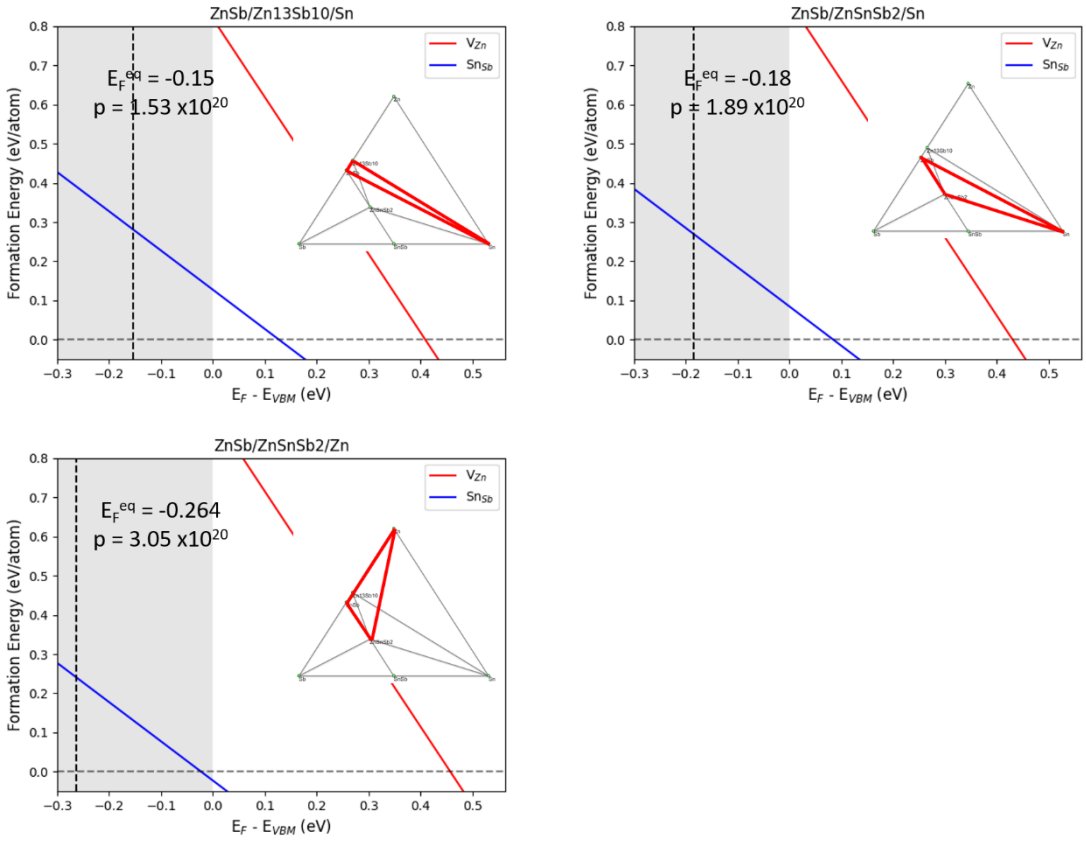


Figure S3. The defect formation energies of the zinc vacancy and Sn dopant on the Sb site, drawn with respect to the three-phase region chosen in each inset. The equilibrium Fermi level and the carrier concentration are shown in each case.